Contents

1 Introduction **1**
- 1.1 The radio sky . . . 1
- 1.2 Active galaxies and the standard model of AGN . . . 3
  - 1.2.1 The zoo of active galaxies . . . 3
  - 1.2.2 Basic ingredients of an AGN . . . 5
  - 1.2.3 The unified scheme . . . 8
- 1.3 A small gallery of radio and X-ray jets . . . 8
  - 1.3.1 Kiloparsec–scale radio and X-ray jets . . . 8
  - 1.3.2 Parsec–scale radio jets . . . 11
- 1.4 NGC 1052 – The star of the show . . . 13

2 Theoretical background **19**
- 2.1 Synchrotron radiation . . . 19
  - 2.1.1 Emission mechanism . . . 19
  - 2.1.2 Spectral distribution . . . 20
  - 2.1.3 The SSC mechanism . . . 21
- 2.2 Jets . . . 22
  - 2.2.1 Jet formation and propagation . . . 22
  - 2.2.2 Jet emission . . . 24
  - 2.2.3 The core–shift . . . 24

3 Observations and data reduction **31**
- 3.1 Fundamentals of radio aperture synthesis . . . 31
- 3.2 Observations of NGC 1052 with the VLBA . . . 33
- 3.3 VLBI data reduction . . . 34

4 Results **49**
- 4.1 Total intensity mapping . . . 49
- 4.2 Model fitting and image alignment . . . 52
- 4.3 Spectral analysis . . . 58
- 4.4 Brightness temperature distribution . . . 70
- 4.5 Polarimetry . . . 76
- 4.6 Core shift analysis . . . 81

5 The big picture **83**

List of Figures

1.1 The radio sky at 408 MHz . . . 2
1.2 Optical spectra of a Seyfert 2 galaxy and a LINER . . . 5
1.3 Sketch of the standard model . . . 7
1.4 Six examples of jets on VLA scales . . . 10
1.5 Cygnus A at radio and X-ray wavelengths . . . 12
1.6 Six examples of pc–scale radio jets taken from the VLBA 2 cm survey . . . 14
1.7 The emission cone in Hα of NGC 1052 and its optical jet . . . 16
1.8 The pc–scale twin jet in NGC 1052 at 22 GHz . . . 18

2.1 Dependence of jet parameters on pressure gradients . . . 26

3.1 An elementary radio interferometer . . . 32
3.2 The antennas of the VLBA . . . 34
3.3 A POSSM plot of one scan after the fringe fitting . . . 37
3.4 The basic path of data *a–priori* calibration in $\mathcal{AIPS}$. . . . 38
3.5 A (u, v)–plot, showing the location of baselines in the (u, v)–plane during the 43 GHz observation of NGC 1052 . . . 39
3.6 Time coverage of the NGC 1052 observation at 43 GHz. . . . 40
3.7 The 43 GHz visibility versus time of the *a–priori* calibrated and the fully edited and self–calibrated data on the baseline FD–PT. . . . 42
3.8 The visibility distribution projected on two perpendicular planes in the (u, v)–plane . . . 42
3.9 Fourier relationship between the brightness and visibility amplitude at 5 GHz 44
3.10 The basic feed self–calibration path in $\mathcal{AIPS}$. . . . 48

4.1 Contour plots of the total intensity flux of NGC 1052 at the observed frequencies . . . 50
4.2 Locations of the various model components on the sky . . . 57
4.3 The aligned model fit maps. . . . 59
4.4 The aligned CLEAN maps. . . . 60
4.5 Spectral index map between 5 and 8.4 GHz . . . 62
4.6 Spectral index map between 8.4 and 22 GHz . . . 63
4.7 Spectral index map between 22 and 43 GHz . . . 64
4.8 Total spectrum of the pc-scale structure of NGC 1052 . . . 65
4.9 The spectra of the four jet regions A,B,C and D. . . . 67
4.10 Spectra of the model fit components in the eastern jet . . . 68
4.11 Spectral indices of the model components . . . 69

4.12 The jet-to-counterjet ratio determined from the fluxes of the model fit components as a function of frequency 70
4.13 Logarithmic representation of the brightness temperature distribution along the eastern jet of NGC 1052 72
4.14 Frequency dependence of the brightness temperatures in the eastern jet of NGC 1052 75
4.15 Calculated opacities along the eastern jet of NGC 1052 77
4.16 Polarized emission images of 3C 345 at 5, 8.4, 22 and 43 GHz 78
4.17 Map of the polarized emission in NGC 1052 at 5 GHz 79
4.18 Slice through the total intensity and polarized emission along the eastern jet of NGC 1052 at 5 GHz. 80
4.19 Image with the model fitting results of the 43 GHz data 81
4.20 Core positions in the two jets at the different frequencies 82

5.1 Model of the central parsecs in NGC 1052 85

Chapter 1

Introduction

1.1 The radio sky

The heavens have always fascinated mankind and inspired poets and artists for ages. Myths have been formed which linked human fate to the stars, and early cultures found their gods manifested in the pictures painted in the sky by the constellations of stars. However, anything that has been discovered during the age of the early astronomy turned out to be just one piece of a much bigger puzzle when scientists began to explore the sky at wavelengths invisible to the human eye. At the beginning of the 20th century it was already recognized that visible light was just one special form of electromagnetic radiation which turns into radio radiation if the waves become longer and into X-rays if the waves become shorter. However, nobody looked for any kind of electromagnetic radiation from space besides the light from the Sun and the stars. We first had to invent artificial radio transmitters before we recognized that the whole sky was already totally populated by them. It was Karl Jansky who found in 1931 that a detectable radio signal in his measurements was extraterrestrial in origin. Later it turned out that the extraterrestrial source of radio radiation which Jansky detected was the center of our own star system, the Milky Way, today called Sgr A.

Today we know what the sky looks like across the spectrum, from the X-ray regime, passing the optical and the infrared to the radio wavelengths. Each wavelength regime that became usable to astronomy after the development of new observing techniques showed new mysteries making the overall picture of the universe we live in even more fascinating than it had been to the naked eye alone before. Figure 1.1 shows the radio sky at 408 MHz (73 cm) in Galactic coordinates (the Galactic Center in the middle). This map of the whole sky is the product of about 15 years of observations between 1967 and 1982 with two radio telescopes in the Northern Hemisphere, located at Effelsberg (Germany) and Jodrell Bank (England), and the Parkes telescope in Australia. It shows the distribution of the galactic synchrotron radiation (see chapter 2.1) across the sky, which is responsible for nearly all of the extended and smooth radiation in the map. In contrast to the optical, where the central region of the Milky Way is completely hidden behind dark clouds, it is clearly visible as the region of the strongest synchrotron emission in the radio regime.

Only a few discrete sources are strong enough to be clearly seen distinct from the extended emission, in contrast to the optical view of the Milky Way being dominated by many stars (discrete sources) and underlaid with some extended emission. Only one of

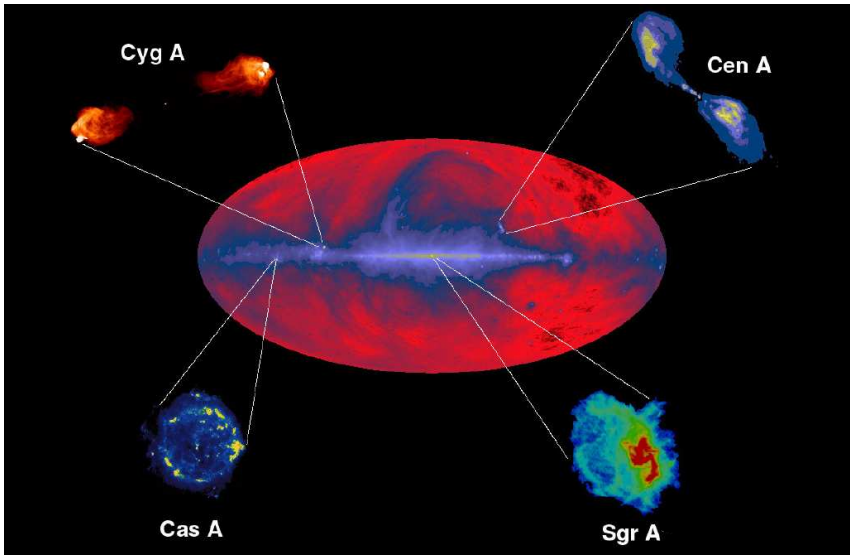

Figure 1.1: The radio sky at 408 MHz (73 cm). The map was produced from the combined data of three radio telescopes, Effelsberg, Jodrell Bank and Parkes taken between 1967 and 1982. The positions of four famous radio sources are indicated: Two radio galaxies, Cygnus A and Centaurus A, a supernova remnant, Cassiopeia A and the center of the Milky Way, Sgr A. The images of Cen A and Cas A are taken from the NRAO image gallery (`www.nrao.edu.imagegallery`). The Cyg A map is shown by courtesy of C. Carilli and the Sgr A image is from Yusef-Zadeh et al. (2000). The 408 MHz all sky map was generated by G. Haslam (MPIfR).

these sources (Cen A) shows structure, all other sources are unresolved, i.e., they appear point–like to a telescope of 70 m[1] in diameter operating at 408 MHz. The resolution of a radio telescope is given by:

$$\Delta\theta = 1.22 \times \frac{\lambda}{D} \tag{1.1}$$

where λ is the wavelength, D is the diameter of the telescope and $\Delta\theta$ is the smallest angular distance which still can be resolved. Thus, in order to find out more about the structure of these sources one had to go to lower wavelengths and/or larger instruments. Although it is technically not possible to build single fully steerable telescopes much bigger than 100 m, the use of interferometric techniques (see chapter 3) allows one to observe with instruments of an effective size of hundreds or even thousands of kilometers. Four of the most prominent discrete sources are shown with higher resolution in Figure 1.1 as they are seen by the Very Large Array (VLA), a connected telescope array of 27 antennas, located in New Mexico, US. Bottom right is a map of the first known extra–solar radio source, Sgr A, which is located at the center of our own galaxy. Bottom left is a map of the strongest discrete radio source visible in the sky, Cas A, a supernova remnant of a star which exploded around 1680. Top left and top right are VLA maps of two radio galaxies, Cyg A and Cen A. Both seem to have a core from which matter is transported along two channels outwards. In usual terminology such a morphology is called a jet. These sources, besides many others, could be identified in the optical regime with galaxies, indicating that there is a process at work which produces very high energies that makes these objects very bright even at these large distances. Radio galaxies are a subclass of the so called

[1] The data of Effelsberg (100 m), Jodrell Bank (76 m) and Parkes (70 m) had to be combined scaling down the resolution of the two bigger telescopes to $0.^{\circ}85$.

active galaxies. Besides the radio galaxies the most important members of this class of objects are the quasars, blazars and Seyfert galaxies. They all show very high–energetic processes, which are confined to a small region at their center. Sometimes the nuclei of these galaxies are a hundred times brighter than their entire starlight. The next section will deal with this "zoo" of active galaxies, introducing the different types of activity and putting them together into a unified scheme.

1.2 Active galaxies and the standard model of AGN

The term active galactic nucleus (AGN) describes a big variety of galactic nuclei, which are unusual compared to classical galaxies in different respects. A common definition is:

> *Active galactic nuclei are nuclei of galaxies which show energetic phenomena that cannot be clearly and directly attributed to stars.*

AGN are peculiar in luminosity, size, spectroscopic properties, variability and morphology. Sometimes an object shows signs of activity only in one respect but generally the phenomenology is more complex. Depending on their properties and the observing techniques used, AGNs were divided in different classes. Often this classification is not unique and there are different labels which can be given to a special object. However, there are a few things nearly all AGN have in common. First, they have a very broad spectral energy distribution (SED) and are thus among the brightest objects in all wavebands. Second, most AGN are strongly variable at all wavelengths and third, they are usually bright X–ray sources. In section 1.2.1 the most common classes of AGN and their similarities and differences shall be introduced. Section 1.2.2 will present the standard model for the underlying physics of AGN and in section 1.2.3 a unified scheme will try to explain the variety of active galactic nuclei with a small number of basic parameters which vary between the different classes, namely their luminosity, age, viewing angle and the so called radio loudness.

1.2.1 The zoo of active galaxies

Quasars and **QSOs** are both artificial words. The first means **qua**si **s**tell**a**r **ra**dio source, the latter **Q**uasi **S**tellar **O**bject. The difference between both terms is mainly historically in nature and is due to the fact that quasars are strong in the radio regime whereas QSOs are not. Nevertheless both names are used somewhat exchangeable as long as the context does not imply a special radio flux. Both classes appear star-like on optical photographs, have very high intrinsic brightnesses, and are usually found at very large distances[2]. For example, the brightest quasar 3C 273 is at a distance of $\sim$700 Mpc and has an optical magnitude of B=13 mag. This corresponds to an intrinsic brightness about a hundred times larger than that of the Galaxy. QSOs show very rich emission spectra with unusually broad lines (up to 10,000 km s^{-1}). These high line widths indicate that the emission comes from regions with a very high velocity dispersion, typical for a dense medium in a deep potential well.

[2]Bright objects are usually very rare. The tendency of quasars to be very far away is thus simply a selection effect due to the fact that rare objects are found predominantly at great distances.

Seyfert galaxies are less luminous than quasars and usually the host galaxy (in most cases a spiral) can be detected. Nevertheless, the core region of the galaxy is unusually bright. Seyfert galaxies are divided in two subclasses. Seyfert 1 galaxies have two sets of emission lines, one with narrow lines with full width at half maximum (FWHM) corresponding to several hundreds of km s^{-1} and additionally very broad lines with widths up to thousands of km s^{-1}. No broad forbidden lines are present. In contrast, Seyfert 2 galaxies only show narrow lines. The common interpretation is that the the broad lines originate in a gas of very high density (n_e=10^9 cm^{-3} or higher) very close to a massive, compact object (see 1.2.2) while the narrow lines originate in a low density gas (n_e=10^3–10^6 cm^{-3}) farther out. This is in agreement with the prediction that forbidden lines originate only in regions with small densities. Very important for unification models (see 1.2.3) was the detection of "hidden" broad line systems in many Seyfert 2 galaxies in polarized light. This is usually explained in terms of an obscuration effect in that the broad line region is hidden behind a central absorber but stays visible in scattered (and thus polarized) light. The transition from Seyferts to quasars is somewhat arbitrary. The strongest Seyfert 2 galaxies for example are brighter than the weakest quasars. This is simply due to the fact that an AGN which shows broad emission lines and appears star like will probably be classified as a quasar whereas it would have been classified as a Seyfert 1 galaxy if in a slightly deeper observation its weak starlight from the surrounding galaxy would had been detected.

LINERs in general are low luminosity AGN (LLAGN) with an optical spectrum similar to Seyfert 2 galaxies, except that the low–ionization lines are relatively strong. LINER is an acronym for **L**ow–**I**onization **N**uclear **E**mission–line **R**egion galaxies. Figure 1.2 shows the optical spectrum of the main target of this work, NGC 1052, which is often called the prototypical LINER, and the Seyfert 2 galaxy NGC 1667. LINERs are very common. They are found in nearly one third of all bright nearby galaxies (Ho et al. 1995). It is not clear if the whole class of LINERs can be seen as the low luminosity extension of the AGN phenomenon. Alternatively, some of the observed LINER spectra may actually be produced as the result of intense star formation[3]. Similarly to the Seyfert galaxies, about 15% of all LINERS show broad components of the Hα line. They can thus also be divided in the subclasses of LINER 1 and LINER 2 nuclei as those sources in which broad Hα lines are detected or undetected, respectively. Whether LINER 2 nuclei in general contain weak broad line systems or not is less clear than for their more luminous counterparts in the Seyfert class. At least in the case of NGC 1052 the broad wings of the Hα line have been shown to be polarized. Therefore, it seems that at least a subset of the LINER class resembles the Seyfert class in this respect.

Radio galaxies are galaxies which emit at radio frequencies. This trivial statement is probably the only definition which can be given in agreement with the various understanding that different people have about this term. Radio galaxies are often defined as galaxies which show radio structure on kpc–scale rather than compact sources, which in turn would be classified as quasars. On the other hand, the detection of an optical galaxy is often

[3]In the case of NGC 1052, however, many independent indicators as the radio jets, the X-ray flux and the detection of broad wings of the Hα line, underline its AGN nature. Additionally, its optical spectrum can well be explained in terms of a simple photoionization model, like in Seyfert galaxies (Gabel et al. 2000).

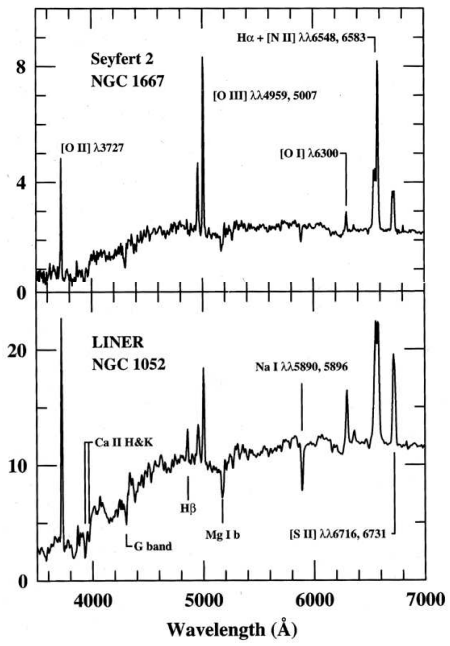

Figure 1.2: The optical spectra of the Seyfert 2 galaxy NGC 1667 and the LINER NGC 1052. Important differences are: The [OIII]/Hβ flux ratio is smaller in LINERs than in Seyfert 2 galaxies, and low–ionization lines ([NII], [SII], [OII] and [OI]) are relatively strong in LINER spectra. Plots taken from Peterson (1997), by courtesy of A. P. Filippenko.

taken as the criterion that turns a quasar into a radio galaxy. Depending on the presence or absence of a broad line system in the optical spectrum, radio galaxies are divided in broad line radio galaxies (BLRG) and narrow line radio galaxies (NLRG). In any case, radio galaxies represent only a small subset of the AGN class since only about 10–15% of all AGN are strong in the radio regime. These are also called radio-loud AGN, in contrast to radio-quiet AGN. A morphological classification is given in section 1.3.2 together with a presentation of the variety of radio sources on parsec– and kiloparsec–scales.

Blazars are radio sources containing a relativistic jet which is directed nearly towards the line of sight to the observer. The beamed jet emission (see section 2.3.1) forms a featureless continuum from the radio regime up to (occasionally hard) X-rays. They can be divided into two subclasses, namely, the BL Lac objects and the core dominated quasars. Emission and absorption lines in BL Lac objects are very weak, if not completely absent. The ones with detected emission lines tend to be at small redshifts. Core dominated quasars often show prominent emission lines which suggest on average higher redshifts. Both show very rapid variability in the optical regime with time scales often smaller than one day.

1.2.2 Basic ingredients of an AGN

In this section the main components of the standard model for AGN is introduced and the observational evidence for the corresponding component will be discussed briefly. Figure 1.3 shows a schematic image of an AGN in the standard model and the relative configuration of its general components.

The central engine – Black hole and accretion disk: Since the detection of AGN, the most fundamental task was to understand what physical mechanism is capable of releasing the enormous energies observed on scales, comparable to the size of the solar system. The only possibility is the accretion of matter onto a very compact object. In this process, the potential energy is converted into kinetic energy, which in turn can be released before the matter reaches the central object. The high observed luminosity (typically 10^{44}–10^{48} erg s^{-1} in luminous quasars) and the small scales derived, for example, from the upper limit on the size of unresolved radio cores of <1 pc provides a simple lower limit on the mass of the accreting object, the Eddington mass. The enormous radiation pressure in the surrounding of the central object requires at least this mass to secure that material in the accretion flow can still be gravitationally bound to the center of the galaxy. For a given luminosity of $L = 10^{46}$ erg s^{-1} it can be estimated that at least a mass of $M_E = 0.8 \cdot 10^8 M_\odot$ is needed to sustain the accretion flow. Such a large value implies that the accreting object could be a black hole.

There is increasing evidence for the presences of black holes in the centers of active galaxies and also in many, if not all, "normal" galaxies. The two major proofs are the measurement of radial and proper motion of stars around the center of our own galaxy at the Sgr A region (Eckart & Genzel 1996) and the detection of a set of moving maser spots in a Keplerian disk in NGC 4258 (Miyoshi et al. 1995). In both cases the derived mass density of the central source argues strongly towards the presence of a black hole of $2.6 \cdot 10^6$ M$_\odot$ in the case of our milky way and $3.6 \cdot 10^7$ M$_\odot$ in NGC 4258.

The accretion flow onto the black hole forms an accretion disk. In this disk, angular momentum is transported outwards by means of viscous friction, and matter is transported inwards. The big amount of released energy is due to the viscous friction, which cools the flow. Alternatively, a large fraction of the gained energy may not be radiated away but be transported with the flow inside the event horizon of the black hole. Obviously, the latter possibility cannot lead to as luminous objects as the former one. For this reason the latter solutions, which are called ADAFs (advection dominated accretion flows) are mainly applicable to low luminosity sources (LINERs, X-ray binaries,...). They have however, big problems in explaining the broadband SED of several objects, especially flat spectrum radio sources, without the inclusion of jets.

In many luminous AGN the optical spectrum exhibits a broad feature, called the big blue bump. This bump can in many cases be well explained by the blackbody radiation of an accretion disk. The absence of this bump in several flat spectrum low luminosity AGN argues towards a combination of a jet model (responsible for the radio emission and probably also the X-ray emission) and an ADAF. This is a very disputed topic and judging the debate is not within the scope of this thesis.

The circumnuclear medium – BLR, NLR and obscuring torus: The region around the putative accretion disk is filled by gas and dust. Three main components seem to describe this AGN surrounding: the broad line region (BLR), the narrow line region (NLR), and a molecular (dusty) torus. Since the emission lines are most likely Doppler broadened, the BLR is expected to be very close to the black hole, exhibiting a big velocity dispersion within the set of different emitting gas components. The NLR is the extension of the BLR at larger distances. In both cases, the volume-filling-factor is $\ll 1$, implying a very filamentary structure of both the BLR and the NLR. Although the BLR is very

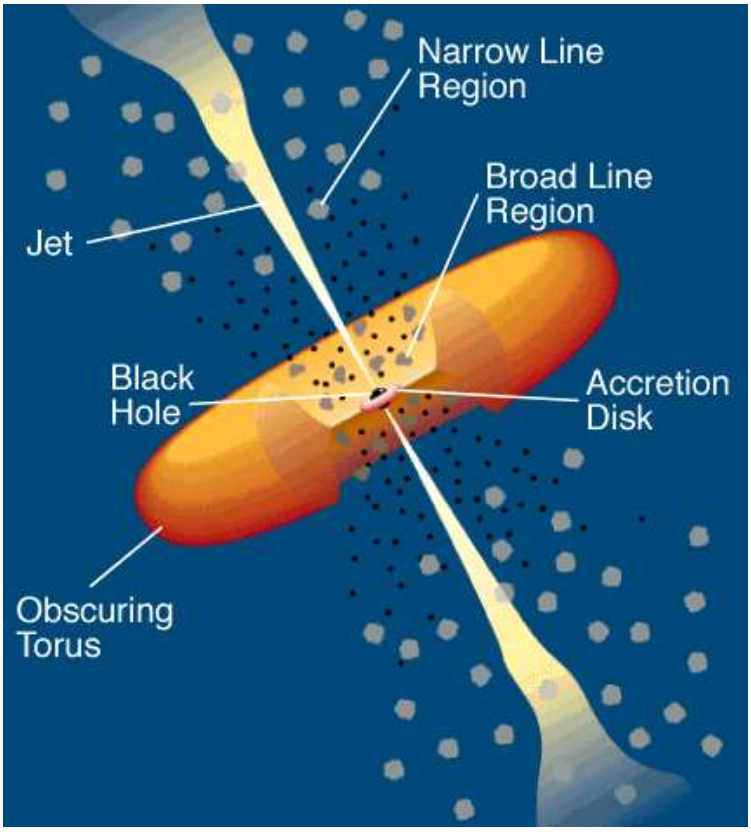

Figure 1.3: Sketch of the standard model, taken from the HEASARC website (`http://guinan.gsfc.nasa.gov`).

compact (smaller than a few tens of lightdays) and presently not resolvable with optical facilities, the NLRs of some AGN have been imaged successfully with the Hubble space telescope (e.g. Falcke et al. 1998). The morphology of the NLR is generally well described by a double–cone emanating from the core of the galaxy.

A small bump in the infrared regime, visible in many AGN spectra, finally suggests the presence of a warm, dusty component. In the unified scheme this dust is usually thought to be ordered in a torus–like structure, possibly being the outer extension part of the accretion disk. Depending on the viewing angle this torus can obscure the BLR, leaving only the emission from the more extended NLR left to observe. Recently, VLBI observations found evidence of such an obscuring absorber, which will be discussed in much more detail in later chapters of this work.

Jets, Hot spots and Lobes: Finally, every AGN is thought to harbor a more or less prominent twin jet, which is emanating perpendicular to the accretion disk. Each of the two jets penetrates the BLR and the NLR, travels on a linear path and finally terminates in a hot spot, the region of interaction between the jet and some kind of surrounding medium. The observed radio lobes represent either a backflow of jet material or the residue of the jet from an earlier epoch. Since these jet components of AGN are the topic of section 1.3 and 2.4, they shall only be listed here.

1.2.3 The unified scheme

With the basic ingredients of the standard model for AGN at hand – namely the supermassive black hole, the accretion disk, the broad and narrow line region, the jet and the obscuring torus – a unified scheme for the different types of AGN can be developed. The phenomenon of a pair of similar types which differ only in the presence or absence of a broad emission line system (Seyfert I/II, LINER I/II, BLRG/NLRG) can be explained with intrinsically only one type each, with the BLR visible or hidden behind the obscuring torus. A viewing angle roughly parallel to the symmetry axis of the torus will make a source appear as a type I object, a line of sight nearly perpendicular to this axis will make the object appear as a type II source. Additionally, this principle can be applied to quasars and radio galaxies. The difference between those is mainly that radio galaxies neither have a BLR nor an UV–bump and the radio cores of quasars are much stronger than in radio galaxies. Applying the same unification principle as above, the BLR and the accretion disk of radio galaxies are hidden behind the torus. In addition, the jet, oriented towards the observer in quasars and perpendicular to the symmetry axis of the torus, becomes Doppler-boosted (see section 2.3.1). In the case of radio galaxies and quasars, as well as for the Seyfert I/II and LINER I/II classes, this simple inclination model reproduces satisfactorily the relative numbers of the corresponding objects. The blazars fit in this scheme as the sources with the jet nearly directly pointing towards the observer. This explains the featureless continuum, since the boosted jet radiation outshines every line feature in the spectrum, as well as the fact that blazars are relatively rare. The small CSS and GPS sources (**C**ompact **S**teep **S**pectrum and **G**iga-Hertz **P**eaked **S**pectrum sources; see section 1.3.2) can be seen as the young radio galaxies and quasars. The remaining differences can be explained in terms of different power and the presence or absence of strong radio emission, the radio loudness.

1.3 A small gallery of radio and X-ray jets

In the previous section we got to know the engines of AGN activity. Now we want to have a look at their "creatures".

Jets are a very common and well studied phenomenon. They occur on very different scales and in various shapes, not only in AGN but also in many Galactic sources where a matter-accreting compact object is involved. This includes young stellar objects (YSOs) as well as nuclei of planetary nebulae, white dwarfs, neutron stars and galactic black holes. A review of galactic jets can be found in Mirabel & Rodríguez (1999). In this section we will focus on the radio and X-ray emission from extragalactic jets.

1.3.1 Kiloparsec–scale radio and X-ray jets

Radio jets on kpc–scale: An extended radio source is typically dominated by the emission from two distinct regions, the radio lobes, which are fed by two jets, emanating from the galactic nucleus. Cyg A (see Figure 1.5) is the standard example for this type of radio sources. The radio lobes extend typically some arcminutes on the sky (corresponding to several hundreds of kpc). The most extreme cases (giants radio galaxies) extend up to some Megaparsec, e.g. 3C 236. Based on their morphology, two separate classes of extended radio sources can be defined. The Fanaroff-Riley class I sources (FR I) exhibit lobes that

become darker and smoother at their ends (edge darkening) and show no prominent hot spots. The FR II sources on the other hand have their brightest regions at the edges and exhibit strong hot spots. Both classes differ in more than just morphology. There is a sharp distinction in the radio luminosity at $5{\cdot}10^{25}\,\mathrm{W\,Hz^{-1}}$ with the FR I sources being less luminous. The steepest spectral indices, indicating optically thin radio emission (see section 2.2.2), occur always at the weaker regions of the lobes, at the edges of the FR I class objects and at inner regions at the FR II sources. The jets are usually less prominent in FR II sources and often seem to be one–sided, an effect of beaming (see 2.1.1) and reduced contrast due to the luminous lobes. The opening angle of the jets tends to be bigger in FR I sources, whereas the FR II jets are better collimated. Figure 1.4 shows some examples of extended radio sources and illustrates the differences between FR I and FR II sources. The physical difference between both classes is generally thought to be the power of the jet and the type of the flow in the jets. The transition may represent a change from a turbulent flow in FR I jets to a supersonic flow in FR II jets.

X-ray emission from jets: Before the launch of the CHANDRA X-ray observatory only a handful of radio galaxies were known to be associated with X-ray emission from the knots or hot spots of jets. Namely, only the jets in Cygnus A, M 87, 3C 120, 3C 390.3, 3C 273, NGC 6251, Pictor A and Mrk 266 were known to be X-ray sources. Additionally, the angular resolution was not sufficient to cross-correlate the detected X-ray jet features directly to the radio morphology. This situation has changed dramatically since July 23rd 1999, the launching day of CHANDRA. Right away the first reported shot at a celestial object, PKS 0637–752, revealed an X-ray jet (Schwartz et al. 2000). This detection was not even expected since PKS 0637-752 was chosen as a moderately strong point source for location of the focus and optical axis of the mirror. Numerous recent publications (see Harris & Krawczynski 2002 for a March 2001 list of jet-related X-ray emission) report about CHANDRA detections of extragalactic and galactic hot spots and other jet features. The 'classical', i.e. pre-CHANDRA X-ray jets have now been imaged in much more detail (see e.g. Figure 1.5). Many well-known radio jets, such as the ones in Cen A or 3C 295 have got their X-ray counterpart. CHANDRA offers the opportunity to study simultaneously the more extended X-ray emitting regions of the jet and the compact nuclear X-ray emission associated with the AGN.

The X-ray emission mechanism is nowadays the matter of hot tempered discussions. The four processes being discussed are:

- **Synchrotron emission from high energy electrons –** In this scenario the electron energies are either spread over a wide enough range to produce the whole emission all the way from the radio to the X-ray regime, or are separated in (at least) two distinct populations, a low energy one producing the radio synchrotron emission and a high energy one for the X-rays. The former possibility can be tested simply by looking at the spectral energy distribution (SED) of the emission. If the X-ray flux exceeds the extrapolated flux from the radio spectrum, using the spectral index of the radio data, this possibility can be excluded. However, the reverse argument is not true. Since the spectral index is expected to become steeper at high frequencies due to energy losses of the high energy electrons, this effect (spectral aging) can cause an overestimation of the X-ray flux by a simple extrapolation of the radio spectrum. If a distinct high energy population of electrons causes the X-ray

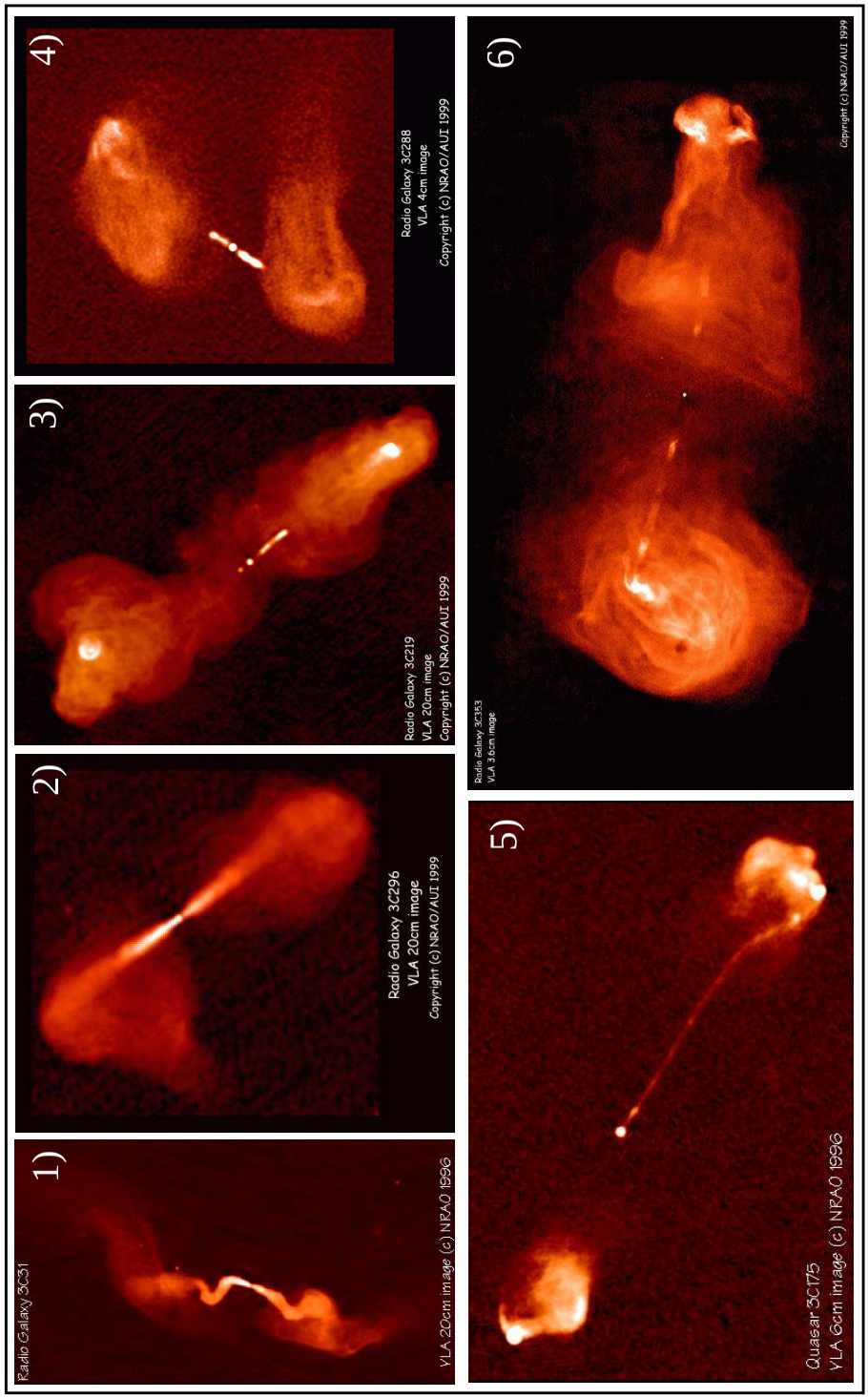

Figure 1.4: Six examples of jets imaged by the VLA (From top left to right bottom): 1) The FR I radio galaxy 3C 31 ($z = 0.0169$; resolution of $5\farcs5$ at 1.4 GHz) has a conical inner jet–counterjet structure and two larger, distorted plumes of emission. 2) 3C 296 is a FR I radio galaxy at z=0.0237 (1.45 GHz map with $4\farcs9$ resolution). 3) 3C 219, a FR II source at z=0.175. The image ($1\farcs4$ resolution, combination of two measurements at 1.4 and 1.6 GHz) shows bright and extended hot spots in both lobes, which extend several hundred kpc. 4) 3C 288, a radio galaxy at z=0.246 shows edge brightening but no prominent hot spots in this 8.4 GHz image ($0\farcs2$ resolution). 5) 3C 175 is a quasar at z=0.768. No counterjet emission is visible at this 4.9 GHz image ($0\farcs35$ resolution). 6) 3C 353 is a radio galaxy at z=0.03 with highly filamentary lobes at 8 GHz ($0\farcs44$ resolution). All images are taken from Alan Bridle's image gallery at the NRAO website.

emission, its mean energy has to be sufficiently higher to match the difference in emitting frequencies (assuming spatial coincidence, i.e. the same magnetic field, see Equation 2.6) and the acceleration event has to have happened more recently since the electrons have not cooled substantially. Single knots in M 87 (Wilson & Yang 2002) could be explained by this model.

- **Thermal emission –** In hot spots the ram pressure of the terminating jet can drive a shock into the surrounding gas. Applying shock jump conditions, it is then possible to estimate the density and temperature of the shocked gas. By comparison with a fitted thermal spectrum this model can be tested. Measurements of the rotation measure in the corresponding region lead to gas densities that can be compared to the predicted values, providing an additional check for thermal models. Hot plasma in an accretion flow could be responsible for the X-ray emission from unresolved cores (see section 2.4.5).

- **Synchrotron self Compton (SSC) emission –** This model has been successfully applied for example to the hot spots of Cygnus A (Harris et al. 1994) and will be described in section 2.3.3. Its main benefit in comparison with the other scenarios is that SSC emission has undoubtly to be produced, since we see the synchrotron emission, while its contribution to the total X-ray flux is not given *a-priori*. It has the problem that the derived values for the magnetic field are well below the equipartition limit (see 2.2.1) given by VLBI measurements of some sources. Note that the equipartition assumption is not given by basic physical principles but is a (well) working hypothesis.

- **External inverse Compton (EIC) scattering of cosmic microwave background photons –** EIC scattering is another process with an uncertain efficiency. In the rest frame of a relativistic jet the cosmic microwave background photons are beamed, enhancing their initially low energy density by a factor D^2 (see Equation 2.11), where D is the Doppler factor of the jet.

None of these processes can explain all observations. Only new observational data and more detailed spectra (as e.g. the X-ray Multi-Mirror Mission (XMM) promises to bring) will solve these questions.

1.3.2 Parsec–scale radio jets

With the development of VLBI (see 3.1) it became possible to resolve the compact radio cores observed in many radio galaxies, as e.g. Cygnus A. The resolution achieved in such experiments is typically about 1 milliarcsecond (mas) depending on the maximal baseline in the VLBI array and the observing frequency. VLBI observations showed that many of the compact radio cores are in fact pc–scale radio jets, apparently the innermost regions of the same jets, which reach out to kpc–scales and feed the lobes of radio galaxies. Additionally, many strong radio sources which show no structure on arcsecond–scales at all, typically quasars in the optical, also turned out to have jet–like morphologies on milliarcsecond–scales giving rise to unification models of radio galaxies and quasars (see 1.2.3).

As a bonus surprise many of these pc–scale jets showed very rapid structural variations. The motions of jet features sometimes appeared to be even faster than the speed of light.

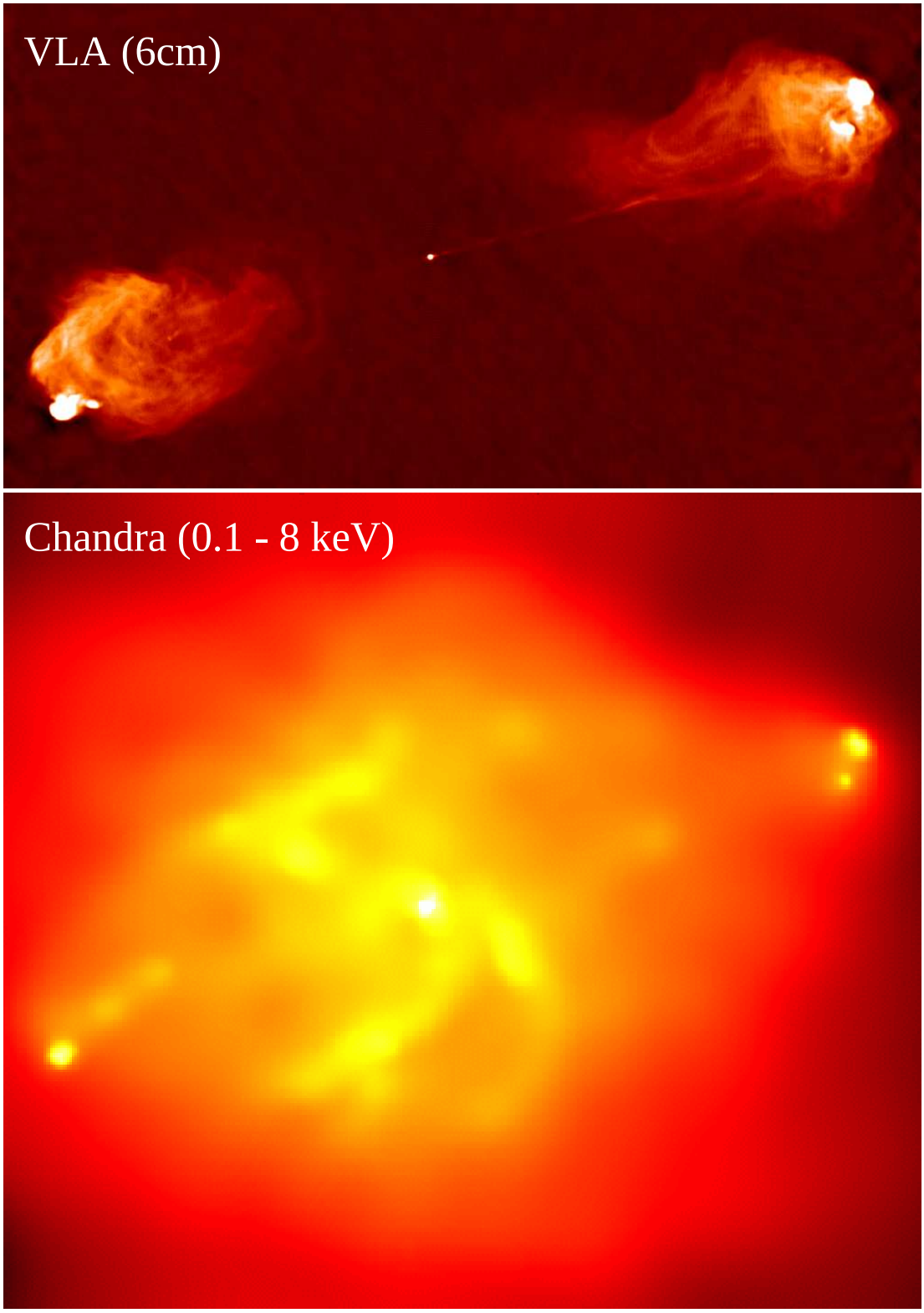

Figure 1.5: Cygnus A at radio and X-ray wavelengths. The upper panel shows a 6 cm ($8.4 \cdot 10^9$ Hz) VLA image (by courtesy of C. Carilli). The lower panel presents a 0.1-8 keV ($2.4–19.2 \cdot 10^{17}$ Hz) CHANDRA image (taken from `http://chandra.harvard.edu/photo/index.html`). Note the 8 orders of magnitude difference in frequency between both images. For a detailed discussion see Wilson et al. (2000), Young et al. (2002) and Smith et al. (2002).

This effect of 'superluminal motion' could be later explained by means of relativistic effects in a special geometry of jet and observer, when small angles to the line of sight and relativistic velocities are involved. During the time interval of the velocity measurement the moving component in the jet then nearly catches up with its own photons, and the measured time difference it takes the component to move perpendicularly to the line of sight appears to be shorter than it really is. The details of this effect can be found for example in (Krolik 1999, page 296).

In contrast to the classical doubles, the pc–scale jets are typically one–sided. The faster a source approaches the observer the stronger its radiation becomes magnified (see Equation 2.4) making the jet on pc–scales appear much brighter than the counterjet (relativistic beaming). These one–sided jets are overrepresented in flux density limited samples (as most surveys of extragalactic radio sources are) and so seem to be more common than their not magnified double–sided counterparts moving mainly in the plane of the sky (Doppler favoritism).

The compactness of some of these sources is proven by flux density variations on time scales of hours (intra day variability (IDV); see Wagner & Witzel 1995). About 30% of all compact flat spectrum sources do present IDV. At present it is not clear whether these variations are intrinsic or due to external scattering. In any case, very compact structures must cause the effect: either smaller than the scattering size of the interstellar medium or of the order of lighthours in size (by light travel time arguments).

Parsec-scale jets can be classified in two groups based on the shape of their radio spectra. Most of them, preferentially the one–sided jets, show nearly flat radio spectra (see Section 2.3.2). Some of the double–sided sources however, exhibit a peak, typically around a few GHz, with a steep decrease of the spectrum above the turnover frequency, similar to the spectra of lobes in radio galaxies. These sources are called GPS (Gigahertz peaked spectrum) sources. If the peak falls below the range of observing frequencies, the source is called a CSS (compact steep spectrum) source.

On this basis, a classification of extragalactic radio sources can be established as follows (adopted from Zensus 1997)

- Luminous core–dominated flat-spectrum sources
- Powerful double–lobed radio galaxies with hot spots (FR II sources)
- Weaker double–lobed radio galaxies without leading hot spots (FR I sources)
- Compact steep–spectrum sources (CSS sources)
- Compact symmetric objects smaller than 1 kpc (CSO sources)

An ongoing effort in studying the sub-milliarcsecond properties of a large sample of radio jets is done in the VLBA 2 cm survey. For this the Very Long Baseline Array (VLBA, see section 3.1.2) has been used since 1994 to image the structure of 171 strong compact sources at 15 GHz with a resolution better than 1 mas. Some images from the survey are shown in figure 1.6.

1.4 NGC 1052 – The star of the show

The main target of this thesis is an elliptical galaxy which has the number 1052 in the New General Catalogue of galaxies. The IAU (B1950.0) name is 0238−084. The Hubble type

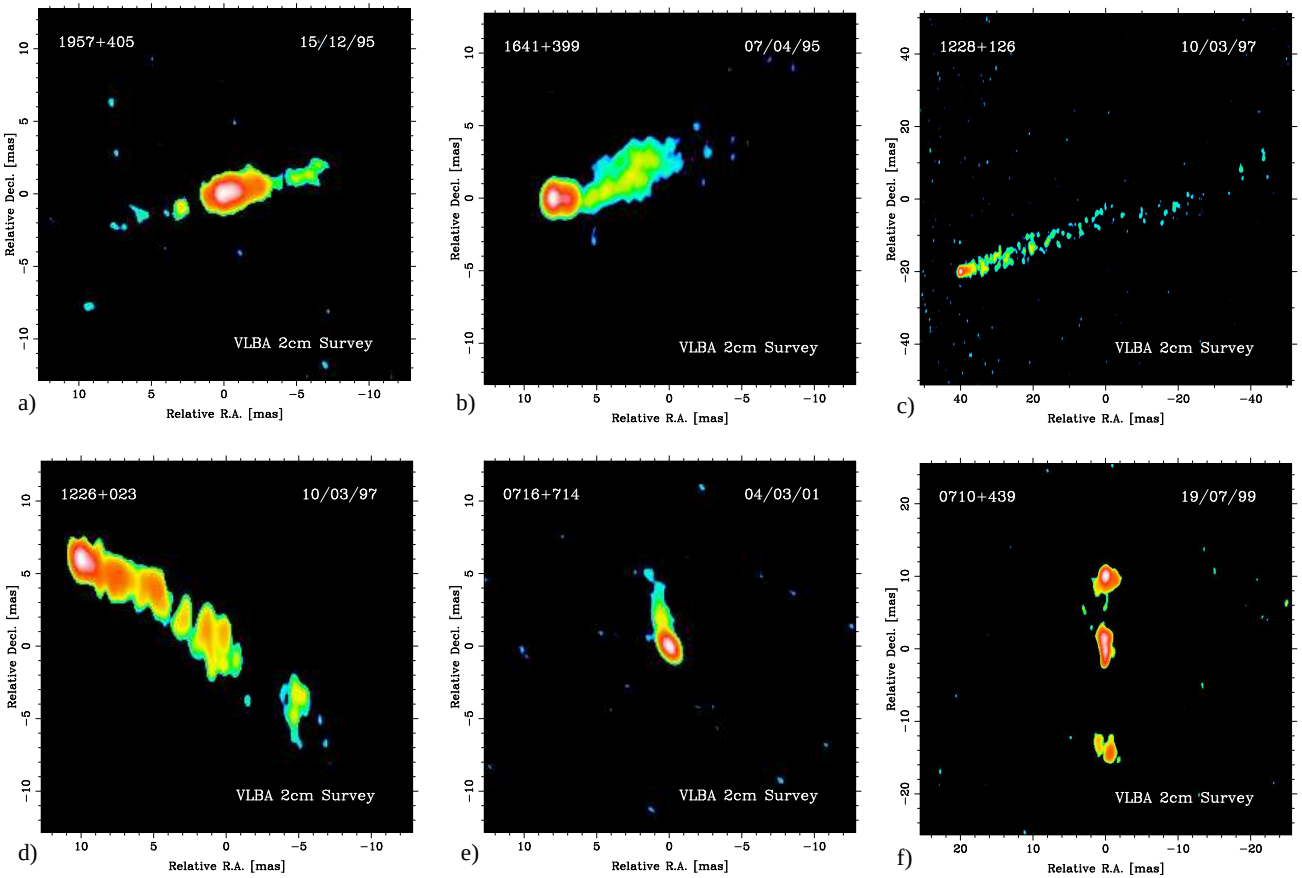

Figure 1.6: Six examples of pc- scale radio jets taken from the VLBA 2 cm survey (Kellermann et al. (1998), Zensus et al. (2002)); a) The core of the prototypical FR II radio galaxy Cygnus A (1957+405) shows a double–sided structure. At 2 cm it contributes less than 1% to the total luminosity of the source; b) The blazar 3C 345 exhibits two distinct regions in its pc–scale jet. At $\sim$ 3 mas distance from the core the well collimated jet with high turnover frequencies turns abruptly into a diffuse jet; c) The jet in M 87 has an apparent kink at about 45 mas from the core; d) 3C 273 was the first detected quasar. Its jet is prominent from radio to x-ray wavelengths; e) 0716+714 is an intra-day variable (IDV) source which shows variations in its flux density of up to 10% within a day. f) 0710+439 is an example of a CSO. Its hot spot advance speed suggests an dynamic age of only a few 1000 years.

of this 12th magnitude object is given as E3 (sometimes as E4). NGC 1052 is the central and dominant galaxy in a small group. Its redshift has been determined to be $z = 0.0049$ (Knapp et al. 1978) corresponding to a distance of 22.6 Mpc (assuming a Hubble constant of $H_0 = 65\,\mathrm{km\,s^{-1}\,Mpc^{-1}}$). This results to a linear scale of $0.11\,\mathrm{pc\,mas^{-1}}$. The proximity of NGC 1052 allows high resolution observations and provides the possibility of exploring relatively weak radiative processes, which would be overlooked in comparable sources at higher redshifts. Table 1.1 summarizes the basic data for NGC 1052.

Optical and infrared properties: The continuum emission in the optical is dominated by starlight with no obvious contribution of a non-thermal component. The optical spectrum of NGC 1052 was found very early (Mayall 1939) to show one of the strongest emission line spectra among elliptical galaxies, which is dominated by low ionization features. Fosbury et al. (1978) showed later that the emission line gas is composed of a luminous central component with a diameter $d \leq 220\,\mathrm{pc}$ and an extended and more diffuse region of $d \sim 2\,\mathrm{kpc}$. The nuclear emission lines are narrow with very weak broad wings in the H_α line (Ho et al. 1997). NGC 1052 can be classified on a spectroscopic base as a Liner 1.9. Barth et al. (1999) found that the broad wings of the Hα line are caused by a broad emission-line in polarized intensity, resembling the hidden type 1 spectra in luminous AGN. This detection is important for two reasons. First, it gives insight into the very vicinity of the putative black hole at the center of the galaxy predicting an obscuring torus which prevents us from seeing the broad line region directly but only in scattered (and thus polarized) emission. Second, it extends the unification scenario established for quasars and Seyfert galaxies to the low luminosity regime. NGC 1052 has a Hα luminosity of $1.26 \cdot 10^{40}\mathrm{erg\ s^{-1}}$, well below the mean value of Seyfert galaxies or quasars.

NGC 1052 is known to have a faint dust lane along the minor axis of the optical ellipsoid (Gallagher 1986) and a central dark cloud towards the nucleus, both too faint to be directly visible in an optical image. Gabel et al. (2000) showed that the measured

Table 1.1: NGC 1052 parameters

Names	NGC 1052, 0238−084, 2E 642
Coordinates (J1950.0)	RA: 02 h 38 m 37.3537 s DEC: -08°28′09.″019[a]
Coordinates (J2000.0)	RA: 02 h 41 m 04.7984 s DEC: -08°15′20.″750[a]
Hubble type	E3/4
Spectroscopic type	LINER 1.9[b]
Redshift	0.0049[c]
Distance	22.6 Mpc[d]
Linear scale	1 mas≙0.11 pc[d]
Flux density at 1.4 GHz	1-1.5 Jy
Bolometric radio luminosity (1-100 GHz)	$4.4 \cdot 10^{40}\mathrm{erg\,s^{-1}}$[e]
Extended radio jet P.A.	95° ± 3° [f]
Parsec–scale jet P.A.	63° ± 6° [g]

[a] Johnston et al. (1995); [b] Ho et al. (1997); [c] Knapp et al. (1978); [d] assuming H_0=65 km s^{-1} Mpc^{-1}; [e] Wrobel 1984; [f] VLA, MERLIN at 1.4 GHz, Wrobel (1984) and this thesis; [g] Kellermann et al. (1998) and this thesis (the error corresponds to the frequency dependence of the P.A. on pc–scales; see chapter 3)

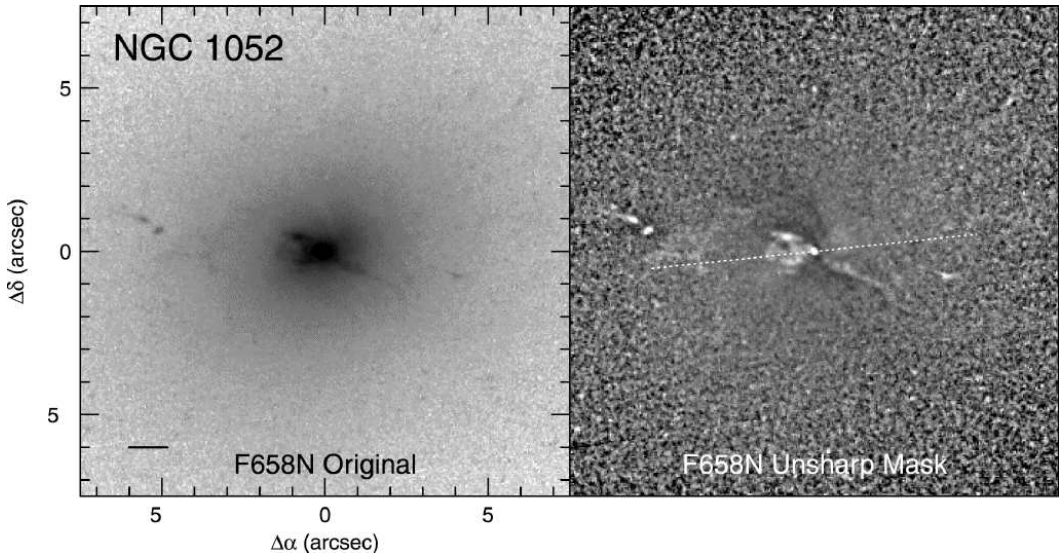

Figure 1.7: The emission cone in Hα of NGC 1052 and its optical jet. Left panel: Hα+ [NII] HST image without continuum subtraction. Right panel: Normalized unsharp masked, residual map of the same data. Absorption regions appear dark and emission bright. The dashed line indicates the axis of the radio jet on kpc–scales. Note the knots of emission, about $5''$ from the core on both sides. Taken from Pogge et al. (2000).

line ratios for Hα/Hβ indicate substantial reddening, with $E(B-V) = 0.42$. They derive that the emission line fluxes can be reproduced well by a simple photo-ionization model. In this model the central power-law ionization source has a spectral index of $\alpha = -1.2$ (flux density $S_\nu \propto \nu^{+\alpha}$) and can also be responsible for the weak high-ionization line system. The gas-covering factor determined from the observed flux distribution agrees with the idea that the line of sight towards the central engine could be obscured. Pogge et al. (2000) reported the presence of a collimated, conical structure in a HST Hα image (see Figure 1.7), probably the NGC 1052 analogon to the emission-line cones known from many Seyfert galaxies. Two knots of emission in the east of the core and one knot in the west indicate a jet-like structure associated with the cone (see Figure 1.7). Recent Keck telescope observations (Forbes et al. 2001) revealed the presence of two distinct globular cluster (GC) sub-populations in NGC 1052. The two populations differ in their color, with a blue and a red population indicating low and high metalicity, respectively. Such a bi-modality in the GC population of early-type galaxies seems to be quite common and suggests that these galaxies might be the product of a merger of two gas–rich spiral galaxies.

NGC 1052 exhibits an infrared excess in its spectrum (see e.g. Becklin et al. 1982), which could be attributed to the central $2''$. This indicates the presence of a dust component, heated by a central non-thermal source.

Radio properties: In the radio regime NGC 1052 is a moderately strong source with a luminosity (integrated between 1 and 100 GHz) of $\sim 4.4 \cdot 10^{40}$erg s^{-1} (Wrobel 1984). It shows a flat or slightly inverted spectrum with a broad peak around 10 GHz and an optically thin decrease in flux density above the peak (e.g. de Vries et al. 1997). The source is variable at all frequencies. At mm-wavelengths, time scales of months and amplitude variations between 0.5 and 2.5 Jy are observed (e.g. Heeschen & Puschell 1983). At longer

wavelengths no continuous monitoring was done but different measurements indicate flux density variations of at least 50% with slightly longer time scales, several months to one year. Heeschen (1970) reported that ∼90% of the radio emission of NGC 1052 originates in a compact core ($< 1.5''$). The extended radio emission, distributed over $\sim 25''$, was imaged by Wrobel (1984) with the VLA at 1.4 and 1.6 GHz. Two lobes east and west of the nucleus contain ∼10% of the total flux density at these frequencies. Both lobes contain regions of enhanced surface brightness, similar to hot spots in more powerful radio galaxies.

Early VLBI observations (e.g. Jones et al. 1984) resolved the core into a nuclear jet with a position angle (P.A.) of $\sim 60°$, in contrast to the $\sim 95°$ P.A. of the extended structure seen in VLA maps. In later VLBI maps the pc–scale structure was found to represent a twin jet with an emission gap between the brighter eastern jet and the western jet (e.g. Kellermann et al. 1998). Exploring the origin of this emission gap is one of the main goals of this thesis. The kinematics of both jets at 2 cm have been investigated by Vermeulen et al. (2002). Observations between 1995 and 2001 show outward motions on both sides of the gap with similar velocities around 0.6 to 0.7 mas yr^{-1} corresponding to $\sim 0.25\,c$. The jets seem to be oriented close to the plane of the sky in order to explain the absence of strong velocity differences due to the Doppler effect. Although the two jets are bent, the trajectories of moving components do not differ significantly from ballistic motion. Kellermann et al. (1999) found free-free absorption towards the western jet, performing multifrequency observations between 0.7 and 21 cm. Kameno et al. (2001) suggested the presence of a pc–scale plasma torus, obscuring the core region of the western jet, from the analysis of multifrequency observations at 2.3, 8.4 and 15.4 GHz. They derived a geometry in which 0.1 pc of the eastern jet and 0.7 pc of the western jet are covered by this torus. Besides this ionized (free-free absorbing) gas component there is also evidence for atomic and molecular gas in the central region of NGC 1052. Claussen et al. (1998) detected H_2O maser emission towards the core of the western jet within the same region which is heavily affected by free-free absorption. The maser spots are ordered in two groups along the jet, rather than perpendicularly to it (like in NGC 4258). The maser line is redshifted with respect to the systemic velocity (see Braatz et al. 1996) corresponding to 100–150 km s^{-1}. It is unusually broad (~ 90 km s^{-1}) and smooth (i.e. not resolved into narrow components). The line varies significantly in shape and velocity with time scales of months. The maser spots seem not to trace a Keplerian disk around the nucleus but show a trend of higher velocities closer to the core. The nature of this maser emission is presently unclear. The masers could originate in the very vicinity of the jet, which is expected to interact strongly with the material in the obscuring torus. Alternatively, they could be the product of an amplification process in a molecular cloud in foreground to the jet (but still within the galaxy or maybe even the torus).

Atomic hydrogen is known to exist in NGC 1052 on various scales. HI in emission was imaged e.g. by Fosbury et al. (1978). Van Gorkom et al. (1986) mapped the distribution of the HI gas with a resolution of $1''$ with the VLA. They report a structure three times the size of the optical galaxy, with an orientation roughly perpendicular to its major axis. The distortion of symmetry in this distribution indicates a recent merger, possibly the same event in that the elliptical galaxy captured the gas. HI absorption is seen against the radio source at the systemic velocity as well as at redshifted velocities. On large scales the gas seems to be ordered in a rotating disk. Recent VLBI observations resolved the HI absorption features towards the nuclear jet (Vermeulen et al. 2002). Different features of a few percent depth can be seen towards the eastern jet. At present it is unclear

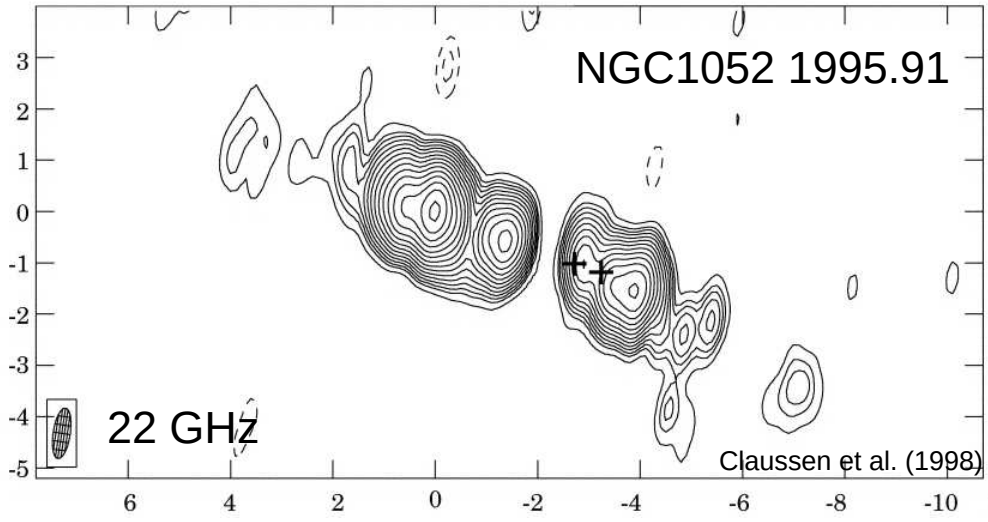

Figure 1.8: The pc–scale twin jet in NGC 1052 at 22 GHz. The contours are -2.9, -1.5, 1.5, 2.9, 4.0, 5.6, 7.8, 10.8, 15.0, 20.8, 29.0, 40.0, 56.0, 78.0, 108.0, 150.9 and 208.0 mJy beam^{-1}. The beamsize is 1.0 × 0.33 mas at a P.A. of -9°. The two groups of water masers are indicated by the two crosses. Taken from Claussen et al. (1998).

whether there is also absorption towards the western jet, that was not seen due to a lack of sensitivity in these observations, as would be expected in the scenario of the western jet being the counterjet. The most prominent absorption feature occurs ∼1–1.5 pc east of the nucleus, interestingly at the same velocity as the maser emission on the other side. Finally, an OH absorption line was also detected by Omar et al. (2002) using the VLA. Future VLBI observations have to explore the distribution of the OH gas on pc–scales.

X-ray properties: NGC 1052 has been detected in X-rays from the satellites Einstein (McDowell 1994), ASCA and ROSAT (Weaver et al. 1999, Guainazzi & Antonelli 1999), Beppo Sax (Guainazzi et al. 2000) and CHANDRA (this thesis). The spectrum of NGC 1052 between 0.1 and 10 keV is very flat (photon index[4] $\Gamma = 0.2 - 1.7$ depending on the applied model) and cannot be modeled with a simple power-law or thermal model. A high column density of absorbing material is needed to model-fit the data. Weaver et al. (1999) derive that the intrinsic spectrum is best described by a power–law that is either (1) attenuated by a two component absorber with $n_{\rm H} = 3 \cdot 10^{23}\,{\rm cm}^{-2}$ and $n_{\rm H} = 3 - 5 \cdot 10^{22}\,{\rm cm}^{-2}$, respectively or (2) Compton-reflected by a high density ($n_{\rm H} > 10^{24}\,{\rm cm}^{-2}$) medium that blocks the direct view to the nuclear source. They calculate 2-10 keV luminosities of $L_{\rm X} = 8 \cdot 10^{41}\,{\rm erg\,s}^{-1}$ and $L_{\rm X} = 2 \cdot 10^{43}\,{\rm erg\,s}^{-1}$ for the two models, respectively. Guainazzi & Antonelli (1999) derived similar models and pointed out that the radial profile of NGC 1052 taken with the HRI camera on board of the ROSAT satellite is not compatible with a point source with an extension going out to 100 arcsec. The broadband spectrum between 0.1 and 100 keV taken with Beppo Sax (Guainazzi et al.

[4]X-ray spectra are usually given in units like photons per keV: $P_{\rm E}({\rm photons\,s^{-1}\,keV^{-1}}) \propto \nu^{-\Gamma}$. Γ is called the photon index. Radio flux densities, on the other hand, are given in energy per unit frequency: $S_\nu \propto P_{\rm E} \times {\rm h}\nu \propto \nu^{-\Gamma+1} \propto \nu^{\alpha}$. The relation between the spectral index α and the photon index is therefore $\Gamma = 1 - \alpha$. To clearly distinguish between both power–law indices, α is sometimes referred to as the energy index.

2000) also yields a high column density and a flat spectrum ($n_H = 2 \cdot 10^{23}\,cm^{-2}$, $\Gamma = 1.4$ for their best model). These authors additionally argue that a thermal bremsstrahlung model can fit the data and that the X–ray luminosity could be due to an advection dominated accretion flow (ADAF).

Bibliography

Barth, A. J., Filippenko, A. V., & Moran, E. C. 1999, Astrophys. J., 515, L61

Becklin, E. E., Tokunaga, A. T., & Wynn-Williams, C. G. 1982, Astrophys. J., 263, 624

Blandford, R. D. & Königl, A. 1979, Astrophys. J., 232, 34

Blumenthal, G. R. & Gould, R. J. 1970, Reviews of Modern Physics, 42, 237

Braatz, J. A., Wilson, A. S., & Henkel, C. 1996, Astrophys. J. Suppl., 106, 51

Brown, R. L. 1987, in Spectroscopy of Astrophysical Plasmas, 35–58

California Institute of Technology. 1991, BAAS, 23, 991

Claussen, M. J., Diamond, P. J., Braatz, J. A., Wilson, A. S., & Henkel, C. 1998, Astrophys. J., 500, L129

Condon, J. J., Condon, M. A., Gisler, G., & Puschell, J. J. 1982, Astrophys. J., 252, 102

Daly, R. A. & Marscher, A. P. 1988, Astrophys. J., 334, 539

de Vries, W. H., Barthel, P. D., & O'Dea, C. P. 1997, Astron. & Astrophys., 321, 105

Eckart, A. & Genzel, R. 1996, Nature, 383, 415

Falcke, H. & Biermann, P. L. 1995, Astron. & Astrophys., 293, 665

Falcke, H., Wilson, A. S., & Simpson, C. 1998, Astrophys. J., 502, 199

Fomalont, E. 1981, Newsletter. NRAO No. 3, p. 3, 1981, 3, 3

Forbes, D. A., Georgakakis, A. E., & Brodie, J. P. 2001, Monthly Not. Roy. Astron. Soc., 325, 1431

Fosbury, R. A. E., Mebold, U., Goss, W. M., & Dopita, M. A. 1978, Monthly Not. Roy. Astron. Soc., 183, 549

Gómez, J. L., Marscher, A. P., Alberdi, A., Jorstad, S. G., & García-Miró, C. 2000, Science, 289, 2317

Gabel, J. R., Bruhweiler, F. C., Crenshaw, D. M., Kraemer, S. B., & Miskey, C. L. 2000, Astrophys. J., 532, 883

Gallagher, J. S. 1986, Publ. Astron. Soc. Pacific, 98, 81

Georganopoulos, M. & Marscher, A. P. 1996, in ASP Conf. Ser. 100: Energy Transport in Radio Galaxies and Quasars, 67

Guainazzi, M. & Antonelli, L. A. 1999, Monthly Not. Roy. Astron. Soc., 304, L15

Guainazzi, M., Oosterbroek, T., Antonelli, L. A., & Matt, G. 2000, Astron. & Astrophys., 364, L80

Harris, D. E., Carilli, C. L., & Perley, R. A. 1994, Nature, 367, 713

Harris, D. E. & Krawczynski, H. 2002, Astrophys. J., 565, 244

Heeschen, D. S. 1970, Astron. J., 75, 523

Heeschen, D. S. & Puschell, J. J. 1983, Astrophys. J., 267, L11

Ho, L. C., Filippenko, A. V., & Sargent, W. L. 1995, Astrophys. J. Suppl., 98, 477

Ho, L. C., Filippenko, A. V., & Sargent, W. L. W. 1997, Astrophys. J. Suppl., 112, 315

Högbom, J. A. 1983, in Indirect Imaging. Measurement and Processing for Indirect Imaging. Proceedings of an International Symposium held in Sydney, Australia, August 30-September 2, 1983. Editor, J.A. Roberts; Publisher, Cambridge, England, New York, USA, Cambridge University Press, 1984, 247

Johnston, K. J., Fey, A. L., Zacharias, N., Russell, J. L., Ma, C., de Vegt, C., Reynolds, J. E., Jauncey, D. L., Archinal, B. A., Carter, M. S., Corbin, T. E., Eubanks, T. M., Florkowski, D. R., Hall, D. M., McCarthy, D. D., McCulloch, P. M., King, E. A., Nicolson, G., & Shaffer, D. B. 1995, Astron. J., 110, 880

Jones, D. L., Tingay, S. J., Murphy, D. W., Meier, D. L., Jauncey, D. L., Reynolds, J. E., Tzioumis, A. K., Preston, R. A., McCulloch, P. M., Costa, M. E., Kemball, A. J., Nicolson, G. D., Quick, J. F. H., King, E. A., Lovell, J. E. J., Clay, R. W., Ferris, R. H., Gough, R. G., Sinclair, M. W., Ellingsen, S. P., Edwards, P. G., Jones, P. A., van Ommen, T. D., Harbison, P., & Migenes, V. 1996, Astrophys. J., 466, L63

Jones, D. L., Wehrle, A. E., Meier, D. L., & Piner, B. G. 2000, Astrophys. J., 534, 165

Jones, D. L., Wrobel, J. M., & Shaffer, D. B. 1984, Astrophys. J., 276, 480

Kameno, S., Sawada-Satoh, S., Inoue, M., Shen, Z., & Wajima, K. 2001, Publ. Astron. Soc. Japan, 53, 169

Kellermann, K. I., Vermeulen, R. C., Cohen, M. H., & Zensus, J. A. 1999, in American Astronomical Society Meeting, Vol. 194, #20.02

Kellermann, K. I., Vermeulen, R. C., Zensus, J. A., & Cohen, M. H. 1998, Astron. J., 115, 1295

Kemball, A. J., Diamond, P. J., & Cotton, W. D. 1995, Astron. &. Astrophys. Suppl., 110, 383

Knapp, G. R., Faber, S. M., & Gallagher, J. S. 1978, Astron. J., 83, 139

Krichbaum, T. P., Alef, W., Witzel, A., Zensus, J. A., Booth, R. S., Greve, A., & Rogers, A. E. E. 1998, Astron. & Astrophys., 329, 873

Krolik, J. H. 1999, Active galactic nuclei : from the central black hole to the galactic environment (Princeton, NJ, USA : Princeton University Press, 1999.)

Leppänen, K. J., Zensus, J. A., & Diamond, P. J. 1995, Astron. J., 110, 2479

Levinson, A., Laor, A., & Vermeulen, R. C. 1995, Astrophys. J., 448, 589+

Lobanov, A. P. 1998, Astron. & Astrophys., 330, 79

Marr, J. M., Taylor, G. B., & Crawford, F. 2000, in Astrophysical Phenomena Revealed by Space VLBI, Proceedings of the VSOP Symposium, held at the Institute of Space and astronautical Science, Sagamihara, Kanagawa, Japan, January 19 - 21, 2000, Eds.: H. Hirabayashi, P.G. Edwards, and D.W. Murphy, Sagamihara, Kanagawa, Japan: Institute of Space and astronautical Science, 2000, 91

Mayall, N. U. 1939, Lick Observatory Bulletin, 497, 33

McDowell, J. C. 1994, in Einstein Obs. Unscreened IPC Data Archive

Mirabel, I. F. & Rodríguez, L. F. 1999, Annu. Rev. Astron. Astrophys., 37, 409

Miyoshi, M., Moran, J., Herrnstein, J., Greenhill, L., Nakai, N., Diamond, P., & Inoue, M. 1995, Nature, 373, 127

Napier, P. J. 1994, in IAU Symp. 158: Very High Angular Resolution Imaging, Vol. 158, 117

Omar, A., Anantharamaiah, K. R., Rupen, M., & Rigby, J. 2002, Astron. & Astrophys., 381, L29

Pearson, T. J., Shepherd, M. C., Taylor, G. B., & Myers, S. T. 1994, in American Astronomical Society Meeting, Vol. 185, #08.08

Peterson, B. M. 1997, An introduction to active galactic nuclei (Cambridge, UK, New York, USA: Cambridge University Press)

Pogge, R. W., Maoz, D., Ho, L. C., & Eracleous, M. 2000, Astrophys. J., 532, 323

Ros, E. 1997, Astrometría diferencial de precisión con VLBI en el triángulo de Draco (y estudios de SN 1993J) (València, Spain: Servicio de Publicaciones, Universitat de València), 35

Rybicki, G. B. & Lightman, A. P. 1979, Radiative Processes in Astrophysics (New York, USA: Wiley-Interscience)

Schwartz, D. A., Marshall, H. L., Lovell, J. E. J., Piner, B. G., Tingay, S. J., Birkinshaw, M., Chartas, G., Elvis, M., Feigelson, E. D., Ghosh, K. K., Harris, D. E., Hirabayashi, H., Hooper, E. J., Jauncey, D. L., Lanzetta, K. M., Mathur, S., Preston, R. A., Tucker, W. H., Virani, S., Wilkes, B., & Worrall, D. M. 2000, Astrophys. J., 540, L69

Smith, D. A., Wilson, A. S., Arnaud, K. A., Terashima, Y., & Young, A. J. 2002, Astrophys. J., 565, 195

Thompson, A. R., Moran, J. M., & Swenson, G. W. 1986, Interferometry and synthesis in radio astronomy (New York, Wiley-Interscience)

Tingay, S. J. & Murphy, D. W. 2001, Astrophys. J., 546, 210

Van Gorkom, J. H., Knapp, G. R., Raimond, E., Faber, S. M., & Gallagher, J. S. 1986, Astron. J., 91, 791

Vermeulen, R. C., Readhead, A. C. S., & Backer, D. C. 1994, Astrophys. J., 430, L41

Vermeulen, R. C., Ros, E., Kellermann, K. I., Cohen, M. H., & Zensus, J. A. 2002, in prep.

Wagner, S. J. & Witzel, A. 1995, Annu. Rev. Astron. Astrophys., 33, 163

Weaver, K. A., Wilson, A. S., Henkel, C., & Braatz, J. A. 1999, Astrophys. J., 520, 130

Wells, D. C., Greisen, E. W., & Harten, R. H. 1981, Astron. &. Astrophys. Suppl., 44, 363

Wilson, A. S. & Yang, Y. 2002, Astrophys. J., 568, 133

Wilson, A. S., Young, A. J., & Shopbell, P. L. 2000, Astrophys. J., 544, L27

Wrobel, J. M. 1984, Astrophys. J., 284, 531

Young, A. J., Wilson, A. S., Terashima, Y., Arnaud, K. A., & Smith, D. A. 2002, Astrophys. J., 564, 176

Yusef-Zadeh, F., Melia, F., & Wardle, M. 2000, Science, 287, 85

Zensus, J. A. 1997, Annu. Rev. Astron. Astrophys., 35, 607

Zensus, J. A., Ros, E., Kellermann, K. I., Cohen, M. H., Vermeulen, R. C., & Kadler, M. 2002, in press (Astron. J., issue August 2002)